7 - 12 SEPTEMBER 2014, KRAKÓW
FORUM ACUSTICUM

Exploring the properties of acoustic particle velocity sensors for near-field noise source localisation applications

Daniel Fernández Comesaña, Emiel Tijs and Hans-Elias de Bree
Microflown Technologies, Tivolilaan 205, Arnhem, the Netherlands.

Summary
One of the main challenges arising from noise and vibration problems is how to identify the areas of a device, machine or structure that produce significant acoustic excitation, i.e. the localisation of main noise sources. Many tools can provide an accurate answer if the geometry is known and the testing process is undertaken in a controlled environment such as an anechoic chamber. Nevertheless, conventional pressure-based source localisation techniques often require a more elaborate, and ultimately more expensive, system to study complex scenarios, without necessarily guaranteeing accurate results. In contrast, the direct visualisation of normal acoustic particle velocity is a robust approach to locating sound sources regardless of frequency range or the reverberation of the measurement environment. This paper introduces the main characteristics of acoustic particle velocity sensors for source localisation purposes. In addition, some practical examples of acoustic mapping are given, demonstrating the theoretical principles introduced.

PACS no. 43.58.-e, 47.80.-v

1. Introduction

Sound visualisation is a powerful tool for investigating a great variety of acoustic and vibro-acoustic problems. It is often necessary to describe not only the location and nature of the sound sources, but also the behaviour of the sound field they generate. The direct representation of the quantity being measured (direct methods) and the application of signal transformations to expand the data acquired (indirect methods) have vastly contributed to the development of the field of acoustic imaging [1].

Near-field measurement performed either by means of scan-based or point-by-point techniques can be used to obtain representation of the sound distribution throughout the space, and ultimately to localise problematic noise sources. The mapping of acoustic quantities provides a simple and effective approach to solve a wide range of problems without traditional frequency constraints imposed by most inverse methods.

Energy wave phenomena around radiating structures can be studied by means of acoustic intensity field visualisation. Using a vector quantity directly acquired by a three dimensional sound intensity p-u probe contributes to a more comprehensive interpretation of acoustic radiation mechanisms. Experimental evidence can be used to understand how the acoustic field is excited, potentially helping to improve the source design or positioning.

This paper is focused upon the assessment of acoustic particle velocity sensors for the localisation and characterisation of noise sources via direct sound mapping. The performance of sound pressure and particle velocity transducers are evaluated in the presence of multiple acoustic excitations. In adittion, the beneficts of acoustic vector fiel mapping using three orthogonal particle velocity sensors in combination with a pressure microphone are shown.

2. Influence of background noise on sound mapping

Sound visualisation techniques often encounter difficulties adapting from controlled experiments to industrial application cases. Laboratory tests are helpful to prove theoretical concepts and demonstrate novel technologies, but the measurement conditions are usually favourable and far different from those in regular industrial scenarios. In most real applications the presence of background noise reduces signal-to-noise ratio, increasing the estimation error and limiting the capabilities for resolving noise sources accurately. Therefore, it is necessary to determine the impact of

extraneous noise sources upon the two fundamental acoustic quantities: sound pressure and particle velocity. In this section, the influence of the background noise is studied by exploring three main concepts: the sound levels perceived close to a sound source, the noise reduction achieved with a directive sensor and the sound field produced in the proximity of a rigid static surface.

2.1. Sound emission

The impact of background noise is relative to the signal emitted by the device under assessment. Near a sound source, the particle velocity level is usually higher than the sound pressure level. This discrepancy is commonly described by their ratio, i.e. acoustic impedance. For a point source in free field, the acoustic impedance can be defined as [2]

$$Z_{point} = \frac{p}{u_r} = \rho\, c \left(\frac{jkr}{jkr+1} \right) \tag{1}$$

where ρ is the air density, c is the speed of sound in air, k is the acoustic wavelength and r is the distance from the source to the measurement position. For far field conditions ($kr >> 1$), Equation 1 becomes the characteristic acoustic impedance of the medium ($\rho\, c$). However, the influence of the imaginary part grows as the distance to the source is reduced, introducing a phase shift between sound pressure and particle velocity. Formulating the above expression in terms of levels[1] yields

$$L_u \approx L_p + 20 \log \left(\left| 1 + \frac{1}{jkr} \right| \right) \tag{2}$$

where L_u and L_p are the acoustic particle velocity and sound pressure level, respectively. Since wavenumber k and source distance r are both positive in this case, Equation 2 shows that the particle velocity level produced by a point source is always larger than the sound pressure level, particularly when $kr < 1$, in the near field.

There are other expressions to model the acoustic behaviour of different sound sources. In the case of a circular piston mounted in an infinite baffle, the on-axis impedance can be expressed as [3]

$$Z_{piston} = \frac{\rho\, c \left(1 - e^{-2j\gamma}\right)}{1 - \alpha e^{-2j\gamma}} \tag{3}$$

where a is the radius of the piston and

$$\alpha = \frac{r}{\sqrt{a^2 + r^2}} \quad , \quad \gamma = k \frac{\sqrt{a^2 + r^2} - r}{2} \tag{4}$$

[1] It should be noted that the standard reference sound pressure is 20 μPa whereas the reference particle velocity is 50 nm/s. The ratio between them approximately equals the characteristic acoustic impedance, i.e. $p_{ref}/u_{ref} \approx \rho c$

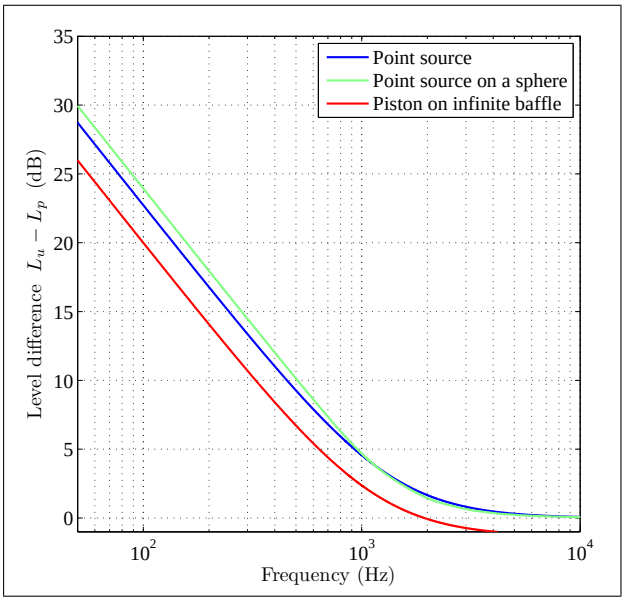

Figure 1. Difference between normal particle velocity and sound pressure levels at 0.04 m from a sound source.

An alternative expression can be used to model a point source encapsulated in a rigid sphere. In practice, this can be achieved by creating a small hole in a hollow rigid sphere driven by a loudspeaker inside it [4]. The on-axis specific acoustic impedance can be defined as [5]

$$Z_{MonopoleB} = -j\rho c \frac{\sum_{m=0}^{\infty} (m + 1/2) \frac{h_m(kr)}{h'_m(kb)}}{\sum_{m=0}^{\infty} (m + 1/2) \frac{h'_m(kr)}{h'_m(kb)}} \tag{5}$$

where b is the radius of the sphere, h_m is the spherical Hankel function of the second kind and order m, and h'_m is its derivative.

The level differences between sound pressure and normal particle velocity can be estimated by using the aforementioned acoustic impedance expressions. These models provide a good approximation of the acoustic behaviour perceived in the vicinity of a sound source although, in practice, more aspects should also be considered, such as complex surfaces, evanescent waves or edge effects.

Since particle velocity level tends to be higher than sound pressure, the inverse form of the acoustic impedance, i.e. the acoustic admittance, is represented instead. Figure 1 shows the simulation results for a measurement distances of 0.04 m, a piston radius of 0.0375 m (3 inch speaker), and a sphere radius of 0.05 m.

It may be surprising that all equations lead to similar results despite the disparity between expressions. As can be seen, the level difference between sound pressure and normal particle velocity is significant in the acoustic near field. The admittance grows proportionally to the source distance and wavelength, the kr product. Therefore, the high particle velocity level

perceived in near field conditions gives particle velocity transducers an advantage over sound pressure microphones for source localisation.

2.2. Sensor directivity

The directional properties of a sensor are linked to the measurement signal-to-noise ratio. Free-field and pressure microphones have a sensitivity response which is not dependent upon the direction of arrival of the incident sound, i.e. they have an omni-directional directivity pattern. On the other hand, particle velocity transducers are equally sensitive to sound arriving from the front or back, but are insensitive[2] to sound arriving from the sides, following a figure-of-eight directivity pattern.

Directivity can be a useful feature for sound source localisation if the sensor is aimed appropriately. The transducer can be steered towards an area of interest to maximise the sound perceived from the aimed direction. For industrial applications, the long reverberation time and the presence of multiple disturbance sources causes the background noise to be distributed fairly homogeneously. As a result, there is an equal probability of sound waves arriving from any direction, condition that precisely defines a "diffuse" sound fields.

Assuming that there are uncorrelated plane waves of equal power arriving at the sensor from all directions, the temporally averaged variance $\overline{\sigma_s^2}$ of the signal output can be calculated by integrating the individual contributions from all directions weighted by the directivity pattern $D(\theta, \phi)$, i.e.

$$\overline{\sigma_s^2} = \int_0^{\pi} \int_0^{2\pi} \overline{\sigma_{PW}^2} D^2(\theta, \phi) \sin(\theta)\, d\phi\, d\theta \qquad (6)$$

where θ and ϕ denote azimuth and elevation angles, respectively. For an omni-directional microphone with unitary gain, Equation 6 simplifies to

$$\overline{\sigma_{omni}^2} = \int_0^{\pi} \int_0^{2\pi} \overline{\sigma_{PW}^2} \sin(\theta)\, d\phi\, d\theta = 4\pi \overline{\sigma_{PW}^2} \qquad (7)$$

On the other hand, the figure-of-eight directivity pattern of a particle velocity transducer can be modelled using the function $cos(\theta)$. Substituting this term into Equation 6 leads to

$$\begin{aligned} \overline{\sigma_{dipole}^2} &= \int_0^{\pi} \int_0^{2\pi} \overline{\sigma_{PW}^2} \cos^2(\theta) \sin(\theta)\, d\phi\, d\theta \\ &= \tfrac{4}{3}\pi \overline{\sigma_{PW}^2} \end{aligned} \qquad (8)$$

The ratio between Equation 7 and Equation 8 defines the effect caused by the directivity in the variance of output signal, thus

$$\overline{\sigma_{dipole}^2} / \overline{\sigma_{omni}^2} = 1/3 \qquad (9)$$

[2] In practice, particle velocity sensors attenuate the sound arriving at the less sensitive direction for about 50 dBs. [6]

The result presented in Equation 9 is in agreement with an alternative derivation introduced in [7]. It shows that, in a diffuse sound field, where uncorrelated wave-fronts arrive homogeneously from all directions, omnidirectional microphones capture three times more energy than transducers with a figure-of-eight directivity pattern. Consequently, the directivity of particle velocity sensors acts as a spatial filter which reduces 66% of the background noise. In terms of sound level, it results in approximately 5 dB improvement in the noise floor of the measurement data.

2.3. Background noise perceived near a rigid boundary

The signal-to-noise ratio plays a key role in the accuracy of acoustic emission estimations. In the absence of background noise, sound pressure and acoustic particle velocity are generally high close to the vibrating areas of a structure, whereas the level is strongly reduced near the rigid sectors. In such a way, the dynamic range is maximised between vibrating and non-vibrating areas. Nonetheless, industrial machinery is often surrounded by other devices which cannot be removed or silenced during the acoustic test. Furthermore, the emitted acoustic energy will be partially reflected back, acting as an additional set of partially correlated sources. The signal-to-noise ratio is therefore greatly reduced, as is the quality of the experimental data. The background noise effectively limits the dynamic range of the sound maps, masking weak sources. It is then desirable to minimise its influence in order to avoid errors in locating the noise emission points.

The sound field produced near a rigid boundary has been simulated to study the impact of background noise upon both sound pressure and normal particle velocity. The rigid surface represents a non-vibrating and fully reflective part of a device, whilst a source produces noise that disturbs the measurements. As it has been mentioned above, the level close to a non-moving surface should be as low as possible to maximize the dynamic range of the sound map. Figure 2 presents the level difference between the sound pressure and normal particle velocity measured with a noise source at one metre distance from the surface and 45° of incidence.

Figure 2 gives quantitative information about how noise generated by external sources can be reduced if particle velocity transducers are used instead of sound pressure microphones. As shown, the main benefit appears at short distances and low frequencies, where the minimisation achieved is higher. At mid and high frequencies it is necessary to measure as close as possible to ensure a reduction in background noise, and to avoid measuring in a region of minimum normal particle velocity.

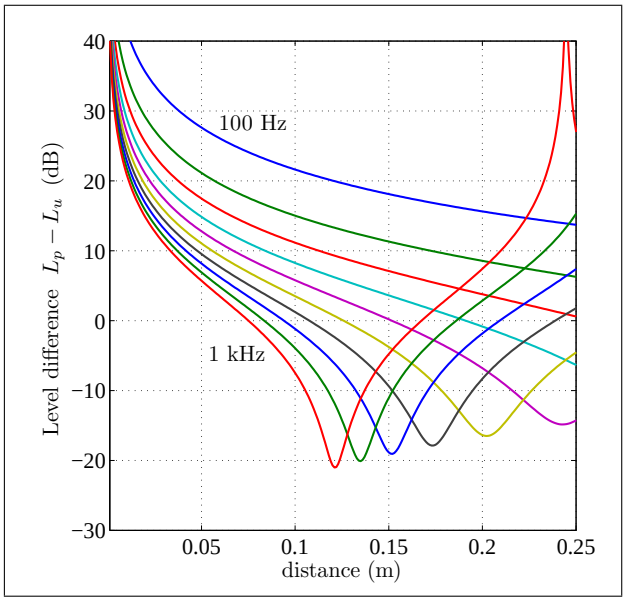

Figure 2. Difference between sound pressure and normal particle velocity levels produced in the vicinity of a rigid surface.

3. Acoustic vector field mapping

The sound energy flow throughout space can be directly captured by means of three-dimensional sound intensity measurements. In the case studied, a three dimensional *p-u* sound intensity probe comprised of a pressure microphone and three particle velocity sensors was used. The instantaneous products of the sound pressure and each orthogonal particle velocity component yields a complex vector: the complex acoustic intensity. The imaginary part of this quantity is known as the reactive intensity **J**, which represents the non-propagating acoustic energy. It is, however, more common to study acoustic sound fields in terms of the active, or propagating, part of the complex intensity [8], i.e.

$$\mathbf{I} = \{I_x, I_y, I_z\} = < p\,\mathbf{u} >_t = \frac{1}{2} Re\{p\,\mathbf{u}\} \qquad (10)$$

where $< . >_t$ indicates time averaging, and the latter expression is based on the complex representation of harmonic variables.

Since both sound pressure and particle velocity are measured simultaneously, the calculation of the three dimensional acoustic intensity can be performed directly, without any approximation. This quantity provides directional information about the flow of acoustic energy. In addition, a scalar term can be extracted for visualisation purposes by taking the modulus of the active intensity vector.

Pressure-based measurement methods cannot be utilised when the pressure-intensity index (the ratio of sound pressure squared to active intensity) is high, which in practice limits the use of *p-p* intensity probes in environments with high levels of background noise or reflections [8]. In contrast, direct intensity measurements using a combination of pressure and particle velocity transducers, the so called *p-u* intensity probes, are hardly affected by this index, enabling the estimation of propagating acoustic energy despite unfavourable conditions [9, 10]. On the other hand, the error of the intensity calculations using *p-u* probes mainly depends upon the reactivity of the sound field (the ratio of reactive to active intensity J/I). If the reactivity is high, for example in the near field of a source, a small phase mismatch in the transducer's calibration may lead to considerable error in the intensity estimate. Although active intensity may be biased in a highly reactive field, the phase difference between pressure and particle velocity can still be measured accurately. Therefore, it is still possible to detect which measurement positions are exposed to an excessive reactivity.

4. Experimental examples

Direct sound mapping techniques, particularly the visualisation of the normal acoustic particle velocity, provide a flexible and robust approach for localising sound sources in a variety of environments. This section presents several practical examples illustrating the results obtained using the scanning technique "Scan & Paint" for direct sound mapping.

4.1. Measurement method: Scan & Paint

The measurement procedure to acquire the data is based upon the scanning technique "Scan & Paint" [11]. The acoustic signals of the sound field are acquired by manually moving a *p-u* intensity probe across a measurement plane whilst filming the event with a camera. In the post-processing stage, the probe position is extracted by applying automatic colour detection to each frame of the video. The recorded signals are then split into multiple segments using a spatial discretisation algorithm, assigning a spatial position depending on the tracking information. Therefore, each fragment of the signal will be linked to a discrete location of the measurement plane. Next, spectral variations across the space are computed by analysing the signal segments. The results are finally combined with a background picture of the measured environment to obtain a visual representation which allows us to "see" the sound. Figure 3 presents a sketch of the measurement methodology.

4.2. Leak detection in building acoustics

A sound field cannot be completely confined to an enclosed space; sound generally propagates throughout air or the structural paths exciting neighbouring rooms. The acoustic features of those rooms are determined not only by the properties of their construction materials but also by the way they are installed.

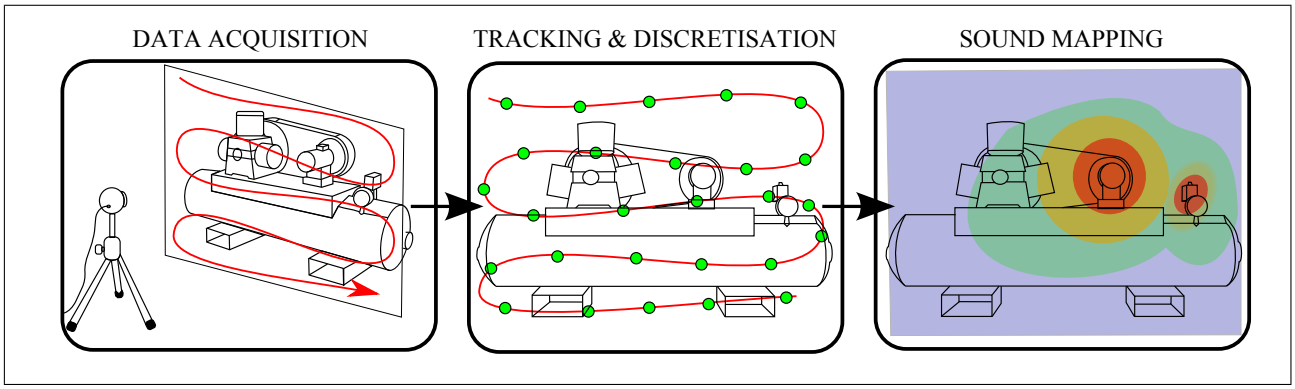

Figure 3. Illustration of the basic steps undertaken with the Scan & Paint measurement method.

Sound insulation losses often appear after the mounting process and should therefore be tested *in situ*.

Two loudspeakers were used to produce a stationary acoustic excitation outside the room being assessed. White noise was used in order excite any possible resonance frequency within the audible range. A 10 minutes scanning measurement was undertaken, moving the probe across an area of 3.2 metres by 1.4 metres approximately 0.03 metres from the surface of the constructive elements. Figure 4 shows experimental examples of leakage detection in constructive materials using a broadband mapping of sound pressure (top) and normal particle velocity (bottom). As can be seen, the spatial distribution of the normal particle velocity has a larger dynamic range than the sound pressure, enabling the localisation of weak noise sources. While the pressure roughly indicates where the noise emission areas are, the normal particle velocity map even reveals the acoustic leakage introduced by the door profile.

In summary, the visualisation of the sound field close to constructive elements can show the distribution of the local excitations, data that can ultimately be used to enhance the acoustic insulation of a room. This experiment demonstrates the high spatial resolution achievable even for large measurement areas in non-anechoic conditions [12].

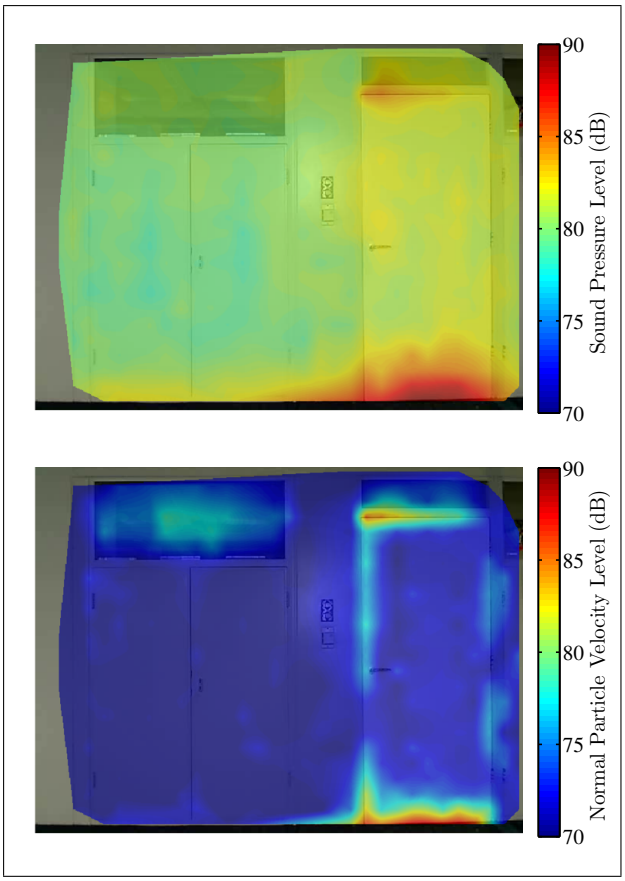

Figure 4. Direct sound mapping for a frequency range between 50 Hz and 10 kHz.

4.3. Loudspeaker in a room

Loudspeaker cabinet design aims to provide the appropriate acoustic loading for the drive units while ensuring a good performance of the complete system [13]. The vibrations induced by the driver frame and moving airmass within the enclosure should therefore be controlled in order to minimise radiation from the cabinet itself. There are several methods for capturing and visualising the vibro-acoustic behaviour of a radiating sound source, but often they are tedious or impractical. In contrast, direct sound field visualisation offers a more flexible approach to display sound phenomena. Figure 5 shows the acoustic sound field at the third octave frequency band of 4 kHz.

It is worth taking the impact of diffracted sound into account to correctly assess the sound emitted by the loudspeaker cabinet. When wavefronts generated at the speaker driver reach the sharp edge of the cabinet there is a sudden increase in the rate of expansion [14]. There are two consequences to this effect. Firstly, part of the acoustic energy radiated effectively turns around the edge and continues propagating in the region behind the plane of the source. Secondly, a new sound wave appears to emanate from the edge, the so called diffracted wave. As a consequence, parti-

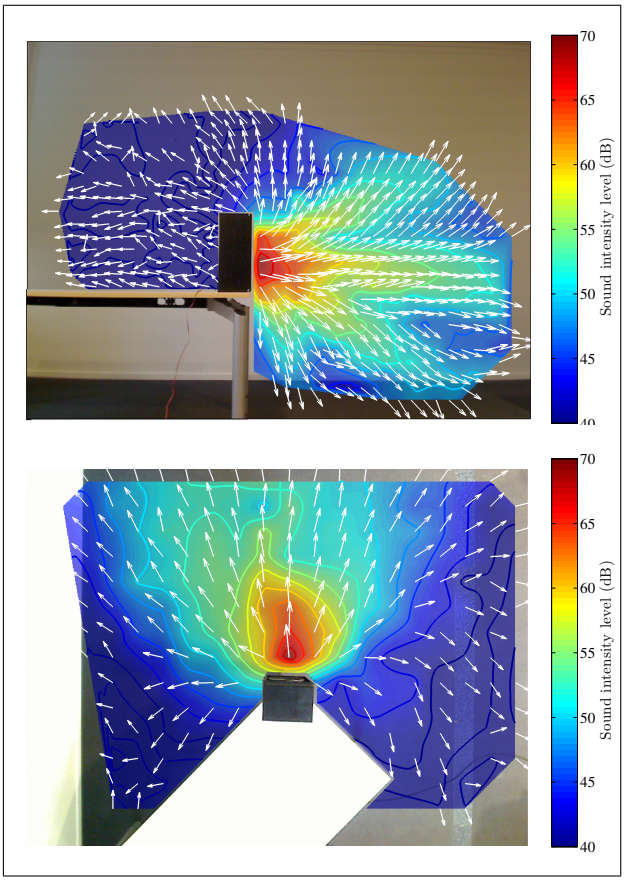

Figure 5. Acoustic intensity vector field of a loudspeaker at 4 kHz.

cle velocity measured on the sides of the loudspeaker is a combination of structure-borne sound radiated by the vibrating cabinet and airborne sound originating from the speaker driver. Additional structural transfer function measurements would be required in order to separate both structure-borne and airborne noise. An extended analysis of this data can be found in [15].

5. Summary

The main characteristics of particle velocity sensors have been studied for source localisation purposes via direct sound mapping methods. It has been proven that external noise sources have little effect on normal particle velocity measurements near a vibrating surface since:

- The particle velocity level caused by vibrating surfaces is higher than the sound pressure level because of near field effects.
- The normal particle velocity close to a non-vibrating structure is very low since it is proportional to the surface displacement, thus achieving a strong reduction in the noise generated by other sources.
- Particle velocity sensors have a figure-of-eight directivity pattern that if pointed towards the vibrating surface reduces the noise contributions from other directions.

Furthermore, experimental evidence using both one dimensional and three dimensional acoustic maps has been presented. It can be concluded that the use of particle velocity sensors in combination with mapping methods can be used for multiple source localisation applications in real-life conditions.

References

[1] R. Beyer, *Sounds of Our Times: Two Hundred Years of Acoustics*. Springer Verlag GMBH, 1999.

[2] F. Jacobsen and P. Juhl, *Fundamentals of General Linear Acoustics*. Wiley, 2013.

[3] K. Beissner, "On the plane wave approximation of acoustic intensity," *The Journal of the Acoustical Society of America*, vol. 71, no. 6, pp. 1406–1411, 1982.

[4] V. Jaud and F. Jacobsen, "Calibration of p-u intensity probes," in *Euronoise 2006*, 2006.

[5] G. Williams, *Fourier Acoustics: Sound Radiation and Nearfield Acoustical Holography*. Academic Press, 1999.

[6] H.-E. de Bree, "The microflown e-book," 2011.

[7] F. Jacobsen and D. tekniske højskole. Laboratoriet for akustik, *The Diffuse Sound Field: Statistical Considerations Concerning the Reverberant Field in the Steady State*. Lyngby. Technical university of Denmark, Acoustics laboratory. Report, Acoustics Laboratory, Technical University of Denmark, 1979.

[8] F. Fahy, *Sound Intensity*. E & FN Spon, 1995.

[9] W. F. Druyvesteyn and H. E. de Bree, "A new sound intensity probe comparison with the pair of pressure microphones intensity probe," *J. Audio Eng. Soc*, vol. 48, no. 1/2, pp. 49–56, 2000.

[10] F. Jacobsen and H.-E. de Bree, "A comparison of two different sound intensity measurement principles," *J. Acoust. Soc. Am.*, vol. 118, no. 3, pp. 1510–1517, 2005.

[11] D. Fernandez Comesaña, S. Steltenpool, G. Carrillo Pousa, H.-E. de Bree, and K. Holland, "Scan and paint: theory and practice of a sound field visualization method," *ISRN Mechanical Engineering*, vol. 2013, no. 241958, pp. 1–11, 2013.

[12] D. Fernandez Comesaña, *Scan-based sound visualisation methods using sound pressure and particle velocity*. PhD thesis, ISVR, University of Southampton, 2014.

[13] J. Borwick, *Loudspeaker and Headphone Handbook*. Focal Press, 2001.

[14] P. R. Newell and K. R. Holland, *Loudspeakers: For Music Recording And Reproduction*. Focal Press, 2007.

[15] D. Fernandez Comesaña, A. Grosso, and K. R. Holland, "Loudspeaker cabinet characterization using a particle-velocity based scanning method," in *AIA-DAGA 2013*, March 2013.